

We are IntechOpen, the world's leading publisher of Open Access books Built by scientists, for scientists

6,900

Open access books available

185,000

International authors and editors

200M

Downloads

Our authors are among the

154

Countries delivered to

TOP 1%

most cited scientists

12.2%

Contributors from top 500 universities



WEB OF SCIENCE™

Selection of our books indexed in the Book Citation Index
in Web of Science™ Core Collection (BKCI)

Interested in publishing with us?
Contact book.department@intechopen.com

Numbers displayed above are based on latest data collected.
For more information visit www.intechopen.com



SQUID Based Nondestructive Evaluation

Nagendran Ramasamy and Madhukar Janawadkar
*Indira Gandhi Centre for Atomic Research, Kalpakkam
India*

1. Introduction

Nondestructive testing (NDT) or Nondestructive evaluation (NDE) refers to techniques, which are used to detect, locate and assess defects or flaws in materials or structures or fabricated components without affecting in any way their continued usefulness or serviceability. The defects may either be intrinsically present as a result of manufacturing process or may result from stress, corrosion etc. to which a material or a component may be subjected during actual use. It is evident that techniques to detect critical flaws before they have grown unacceptably large are of vital importance in the industry for in-service inspection, quality control and failure analysis. There are several NDE techniques of which one of the widely used techniques is based on eddy currents. However, the conventional eddy current technique has the drawback that it can detect flaws upto a certain depth under the surface of the conducting specimen under investigation and is not suitable for locating deep subsurface defects. Such limitations can often be overcome with the use of high sensitivity SQUID sensor. Nondestructive evaluation of materials and structures using low temperature SQUID (LTS) as well as high temperature SQUID (HTS) has been proposed and the potential of the technique has been demonstrated during the last two decades (H. Weinstock, 1991 & G.B. Donaldson et al, 1996). The SQUID based NDE offers many advantages such as high sensitivity (~ 10 to 100 fT/ $\sqrt{\text{Hz}}$), wide bandwidth (from dc to 10 kHz), broad dynamic range (>100 dB) and its intrinsically quantitative nature; disadvantage of this technique is that the SQUID sensor operates only at cryogenic temperatures which makes it relatively expensive. However, despite the expensive cryogen and associated inconvenience in handling, SQUID sensors find a niche in areas where other NDE sensors fail to achieve the required performance (H.-J. Krause & M.V.Kreutzbruck, 2002).

The SQUID based NDE systems have been developed and utilized in several areas of application. At university of Strathclyde, system based on SQUID sensor has been used for the detection of flaws in steel plates (R.J.P. Bain et al., 1985, 1987; S. Evanson et al., 1989). Weinstock and Nisenoff were the first to demonstrate the possible use of SQUID sensors for the study of stress - strain behaviour in a ferromagnetic material (H. Weinstock & M. Nisenoff, 1985, 1986). The SQUID sensors have been used for the detection of tendon rupture in pre-stressed steel tendons of concrete bridges through magnetic flux leakage method (G. Sawade et al., 1995; J. Krieger et al., 1999). Marco Lang et al evaluated the fatigue damage of austenitic steel by characterizing the formation of martensite due to quasi-static and cyclic loading with the help of the SQUID based measuring instrument (M. Lang et al., 2000). SQUID sensors have been successfully used for the detection of ferrous inclusions in

aircraft turbine discs by Tavrin et al. (Y.Tavrin et al., 1999). The presence of such inclusions may initiate cracks in these critical parts and may eventually lead to failure. The magnetic inclusions in the nonmagnetic alloy of the turbine discs have been investigated by pre-magnetizing the turbine discs and probing their remanent field using the SQUID sensor. Since the sensitivity of the SQUID is very high (under $5 \text{ fT}/\sqrt{\text{Hz}}$) and remains constant down to frequencies as low as 1 Hz, these sensors are widely utilized for the detection of deep sub-surface flaws in conducting materials through low frequency eddy current excitation to take advantage of increased skin depth at low frequencies. The SQUID based eddy current NDE technique plays a major role in detecting deep subsurface defects embedded in thick multilayered aluminum structures used in aircraft lap joints.

In this chapter we describe the working principle of the DC SQUID sensor, schemes generally used to couple an external signal to the SQUID sensor, construction of a SQUID-based NDE system by using a low temperature DC SQUID sensor and its associated readout electronics developed in our laboratory. The SQUID system in our laboratory has been used for the measurement of deep subsurface flaws by inducing eddy currents in conducting materials at relatively low frequencies. Detailed experimental studies have been carried out for the determination of optimum eddy current excitation frequencies for the flaws located at different depths below the top surface of an aluminum plate. This system has also been used for the measurement of extremely low content of magnetic δ - ferrite in the 316L(N) stainless steel weldment specimens subjected to high temperature low cycle fatigue (LCF).

2. SQUID sensor

The SQUID (Superconducting Quantum Interference Device) is an extremely sensitive sensor for magnetic flux and its output voltage is a periodic function of applied magnetic flux with the periodicity of one flux quantum Φ_0 ($= h/2e = 2.07 \times 10^{-15} \text{ Wb}$). To utilize the SQUID sensors for real applications, Flux Locked Loop (FLL) readout electronics has been developed in our laboratory to linearise the periodic output voltage of the SQUID. By using SQUID sensor and its associated readout electronics, it is possible to detect a change in applied magnetic flux whose magnitude is much less than one flux quantum. SQUID sensor can measure any physical quantity that can be converted into magnetic flux, and has been used, for example, for the measurement of magnetic field, magnetic field gradient, magnetic susceptibility, electric current, voltage, pressure, mechanical displacement etc. with an unprecedented sensitivity. The systems based on SQUID sensors offer a wide bandwidth (from near dc to hundreds of kHz), wide dynamic range (>100dB) and an intrinsically quantitative response. The unprecedented sensitivity of the SQUID sensor together with the use of superconducting pickup loops (used as input circuits) enables one to realize practical measuring instruments for the measurement of extremely weak magnetic signals with a high sensitivity.

2.1 Principle of operation

The SQUID is basically a superconducting sensor, which operates below the superconducting transition temperature (T_c) of the superconducting materials used for the fabrication of the device. The basic phenomena governing the operation of SQUID devices are flux quantization in superconducting loops and the Josephson effect (fig.1.). While

detailed descriptions are available in the literature (J. Clarke, 1993; H. Koch, 1989), a brief description of the working principle of the SQUID sensor is included here to make this chapter self-contained.

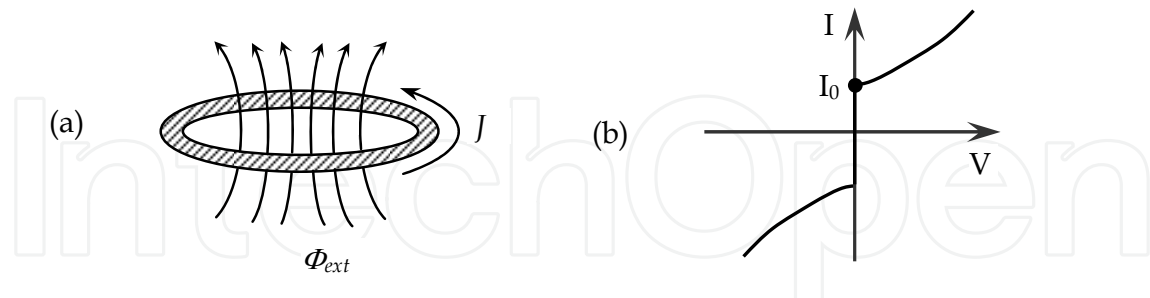


Fig. 1. (a) Flux quantization. (b) Non hysteretic I-V characteristic of a resistively shunted Josephson junction

Flux quantization refers to the fact that the total flux linked with a superconducting loop is always constrained to be an integral multiple of a flux quantum (Φ_0).

$$\Phi_{tot} = \Phi_{ext} + LJ = n\Phi_0 \quad (1)$$

where Φ_{ext} is the externally applied magnetic flux, L is the self inductance of the superconducting loop, J is the screening current induced in the superconducting loop because of the application of the external magnetic flux and n is an integer. The Josephson effect refers to the ability of two weakly coupled superconductors to sustain at zero voltage a supercurrent associated with the transport of Cooper pairs, whose magnitude depends on the phase difference between the two superconductors.

$$I = I_0 \sin \delta\varphi \quad (2)$$

where I_0 is the maximum current the junction can sustain without developing any voltage and is known as critical current of the Josephson junction and $\delta\varphi$ is the phase difference between the two weakly coupled superconductors. When two superconductors are separated by a very thin oxide barrier (tunnel junction), the establishment of tunneling assisted phase coherence leads to Josephson effect; I-V characteristic of such a tunnel junction shows hysteretic behaviour due to non-negligible value of junction capacitance. This hysteresis is, however, undesirable and can be eliminated by shunting the junction with appropriate on-chip thin film resistor to provide sufficient damping of the phase dynamics. A DC SQUID consists of two such non-hysteretic Josephson junctions connected by a superconducting loop.

To describe the operation of the dc SQUID, we assume that the bias current I_b is swept from zero to a value above the critical current ($2I_0$) of the two junctions. An external magnetic flux varying slowly in time is applied perpendicular to the plane of the loop. When the external applied magnetic flux is zero (or $n\Phi_0$, n is an integer), there is no screening current induced in the superconducting loop and the bias current I_b simply divides equally between the two junctions assuming the SQUID to be symmetric. When external magnetic flux Φ_{ext} is applied, the requirement of flux quantization generates a screening current $J = -(\Phi_{ext} - n\Phi_0)/L_s$, where L_s is the inductance of the SQUID loop and n is an integer which makes the

value of $n\Phi_0$ to be nearest to the applied flux Φ_{ext} . The screening current induced in the SQUID loop adds to the bias current flowing through junction 1 and subtracts from that flowing through junction 2. When the junction 1 reaches its critical current $I_0 = I_b/2 + J$, the current flowing in junction 2 is $I_b/2 - J$ (that is, $I_0 - 2J$) and the total current flowing in the SQUID is $2I_0 - 2J$. At this point the SQUID switches to the non-zero voltage state. When the applied flux is increased to $\Phi_0/2$, the screening current J reaches a value of $\Phi_0/2L_s$ and the critical current falls from $2I_0$ to $2I_0 - (\Phi_0/L_s)$ as shown in fig.2 (b). When the flux Φ_{ext} is increased further the SQUID makes a transition from the flux state $n = 0$ to $n = 1$, J changes its sign and reaches zero again when Φ_{ext} becomes equal to Φ_0 . At this point, the critical current of the SQUID is restored to its maximum value of $2I_0$. In this way the critical current oscillates as a function of Φ_{ext} . If we bias the SQUID with a dc current greater than the critical current of the two Josephson junctions, the voltage developed across the SQUID oscillates with a period of Φ_0 when the input magnetic flux steadily increases. Thus, the SQUID produces output voltage in response to a small input flux $\delta\Phi$ ($\ll \Phi_0$), and is effectively a flux to voltage transducer. The voltage swing δV produced at the output of the SQUID when the flux changes from $n\Phi_0$ to $(n + 1/2)\Phi_0$ is known as the modulation depth of the SQUID. The modulation depth of a typical low T_c DC SQUID based on Nb/AlO_x/Nb Josephson junctions is ~ 20 to $30 \mu\text{V}$. The modulation depth δV is maximum for bias currents a little above the maximum critical current of the SQUID, and during operation the SQUID is tuned to the bias current at which the modulation depth is a maximum.

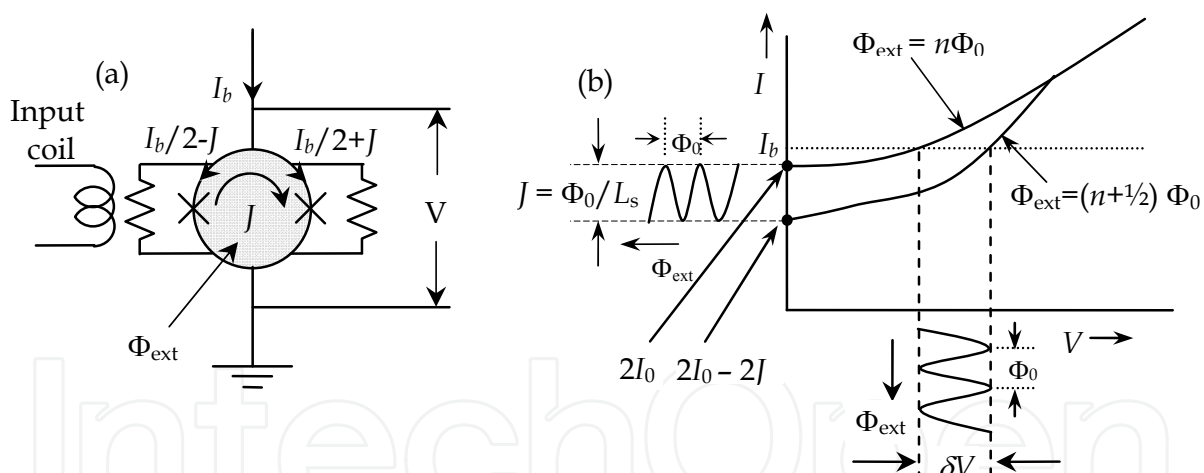


Fig. 2. (a) dc SQUID (b) I-V characteristic of the dc SQUID with the application of input magnetic flux.

3. Flux Locked Loop (FLL) readout electronics

The periodic output voltage of the SQUID allows the SQUID to be operated in a small signal mode around the optimum working point but the linearity of response is limited to flux range much less than $\Phi_0/2$. The small signal readout can only be used when the amplitude of variation of magnetic flux signal is limited to the linear range around the working point ($\ll \Phi_0/4$). However, in most of the applications, the signal flux, which is required to be measured, varies from a fraction of a flux quantum to several hundreds of flux quanta.

Therefore, the measurement system based on the SQUID sensor should be designed to provide a wide dynamic range as required in any application. In order to linearise the periodic output voltage, the SQUID should be operated in a feedback loop as a null detector of magnetic flux; the voltage at the output of the readout electronics will then be proportional to the input signal flux. In order to suppress the $1/f$ noise and dc drifts in the preamplifier the signal of interest is shifted to frequencies well above the threshold of $1/f$ noise by using high frequency flux modulation scheme. The flux modulation scheme is illustrated in fig.3. In this scheme, the signal flux, $\delta\Phi_{\text{sig}}$ which is to be measured is modulated by a high frequency carrier flux $\Phi_m(t)$. The sinusoidal modulation flux, $\Phi_m(t)$ of frequency f_m with a peak-to-peak value of nearly $\Phi_0/2$ is applied to the SQUID. When there is no applied signal flux or the applied input flux is $n\Phi_0$, the SQUID produces output voltage with a frequency twice the frequency of the modulation flux $\Phi_m(t)$ and there is no component at the modulation frequency present in this output. When this voltage output is fed to a lock-in detector referenced to f_m , the output of the lock-in detector is zero. On the other hand, when the applied signal flux is $(n+1/4)\Phi_0$, the SQUID output voltage has a component at frequency f_m , which is in-phase with the carrier frequency and the output of the lock-in detector is a maximum. Similarly, when the signal flux is $(n-1/4)\Phi_0$, the SQUID output voltage has a component at frequency f_m , which is out of phase with the carrier frequency and the output of the lock-in detector has a maximum negative value. Thus, as one increases the flux from $n\Phi_0$ to $(n+1/4)\Phi_0$, the output from the lock-in detector referenced to f_m steadily increases from zero to a maximum positive value; if instead the flux is decreased from $n\Phi_0$ to $(n-1/4)\Phi_0$, the output from the lock-in detector referenced to f_m decreases from zero to a maximum negative value. The lock-in output is integrated and fed back to the same coil as that used for flux modulation via a feedback resistor. The signal flux $\delta\Phi_{\text{sig}}$ applied to the SQUID produces an output of $-\delta\Phi_{\text{sig}}$ from the feedback loop to maintain a constant flux in the SQUID, while producing an output voltage across the feedback resistor, which is proportional to $\delta\Phi_{\text{sig}}$.

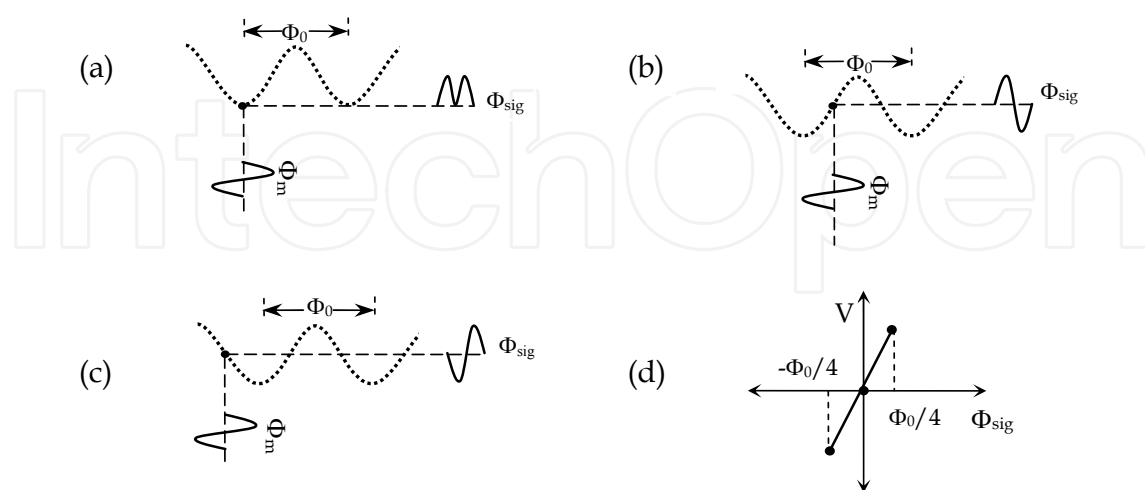


Fig. 3. Schematic representation of flux modulation scheme when the signal flux is at (a) $n\Phi_0$, (b) $(n+1/4)\Phi_0$ and (c) $(n-1/4)\Phi_0$. (d) Linearized output as the signal flux varies from $(n-1/4)\Phi_0$ to $(n+1/4)\Phi_0$.

The schematic diagram of the FLL readout electronics is shown in fig.4. In order to achieve a low system noise, it is necessary to match the output impedance of the SQUID device and input impedance of the preamplifier. LT1028 (Linear Technology) was chosen to construct the preamplifier. The spectral density of the voltage noise (e_n) and current noise (i_n) of the preamplifier at a frequency of 100 kHz are specified by the manufacturer to be about $0.9 \text{ nV}/\sqrt{\text{Hz}}$ and $1 \text{ pA}/\sqrt{\text{Hz}}$ respectively. The optimum input impedance (e_n/i_n) of the preamplifier is, therefore, about 900Ω . Since the dynamic resistance of the SQUID at its optimum bias point is about 1Ω , one requires a coupling circuit with an impedance transformation of about 900 for effective signal extraction from the SQUID. In addition, the bandwidth of the coupling circuit should be as large as possible to extract the 100 kHz modulation signal without attenuation. For this, a room temperature step up transformer with a turns ratio of 30 has been fabricated and used as an impedance matching circuit. The room temperature transformer consists of 10 turns of 24 SWG copper wire as primary coil and 300 turns of 28 SWG copper wire as secondary coil wound on a toroidal ferrite core. The inner and outer diameters of the toroidal core are 10 mm and 18 mm respectively. The step up transformer is housed in the preamplifier box and the preamplifier is mounted at the top of SQUID insert. The SQUID is biased with an optimum dc bias current, I_b to get maximum voltage modulation from the SQUID sensor. The magnetic flux, which is to be measured (in actual measurements) is applied to the input coil of the SQUID, which is inductively coupled to the SQUID loop via the mutual inductance, $M_i \propto \sqrt{L_i L_s}$, where L_i is the self inductance of the input coil and L_s is the self inductance of the SQUID loop. The signal flux is modulated by a 100 kHz sinusoidal flux whose peak-to-peak amplitude is less than $\Phi_0/2$. The modulated output voltage from the SQUID is stepped up by the impedance matching transformer and further amplified by a two stage amplifier with sufficient gain and fed to the signal input channel of the analog multiplier. The modulated output is phase sensitively detected with respect to the reference signal supplied from the same 100 kHz oscillator to

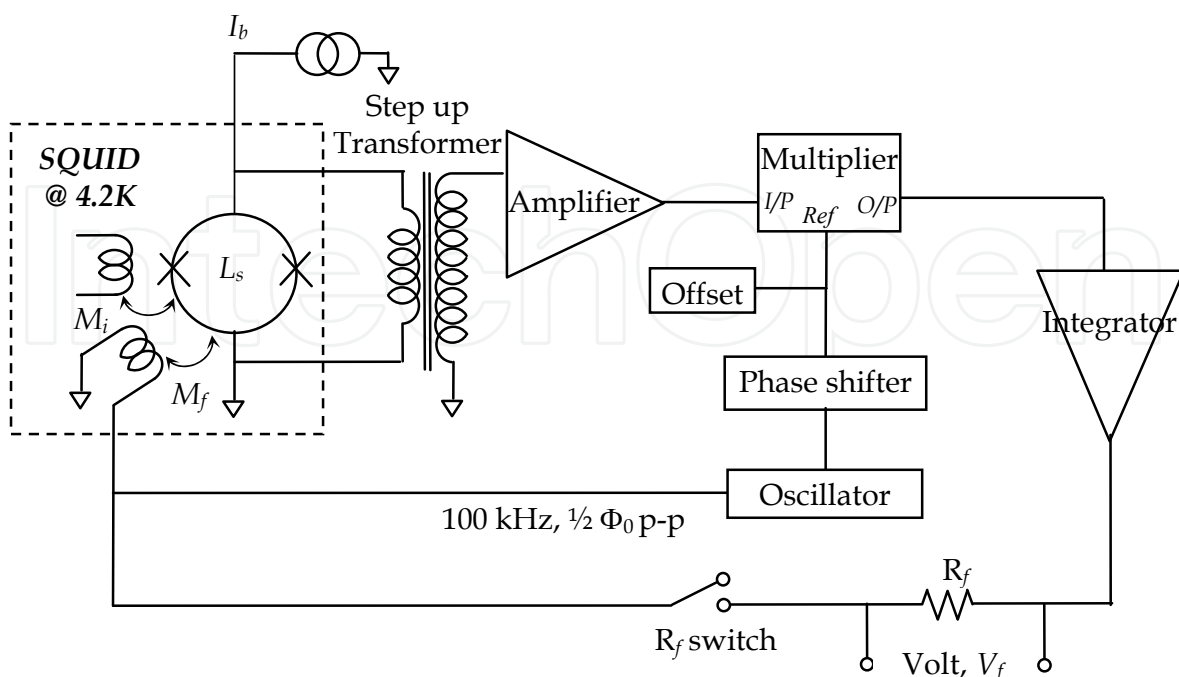


Fig. 4. Schematic diagram of the flux locked loop electronics with flux modulation scheme.

the reference input channel of the analog multiplier. The output of the analog multiplier is integrated and fed back as a current to the feedback coil in order to counterbalance the signal flux applied to the SQUID. The voltage, V_f developed across the feedback resistor R_f is proportional to the input flux and the transfer function of the system ($\partial V_{FLL}/\partial \Phi_{sig}$) is given by (R_f/M_f) , where R_f is the feedback resistance and M_f is the mutual inductance between the feedback coil and SQUID (J. Clarke et al., 1976). When the feedback switch is closed, the feedback flux at the SQUID cancels the input flux and the system uses the SQUID as a null detector of magnetic flux. The voltage developed across the feedback resistor is proportional to the applied input flux and the time variation of this voltage is an exact replica of the time variation of the input signal flux coupled to the SQUID. The system gain can be varied by simply varying the value of the feedback resistor. The figures of merit of the SQUID system with the FLL readout electronics are the flux noise, slew rate and bandwidth; these values are listed in table 1 for the system developed in our laboratory.

Flux noise ($\mu\Phi_0/\sqrt{\text{Hz}}$)	Slew rate (Φ_0/s)	Bandwidth (kHz)
10	5×10^5	10

Table 1. Benchmarks of the SQUID system

4. Important issues in building SQUID based measuring systems

There are some important issues to be considered while designing and building measuring instruments based on SQUID sensors. Since the sensing area of the SQUID is very small (typically 10^{-2} mm^2), direct sensing of the signal flux leads to poor field resolution. The field resolution can be improved to some extent by increasing the effective area of the SQUID sensor's square washer (J.M. Jaycox & M.B. Ketchen, 1981). A better way to increase the field resolution, however, involves the use of superconducting pickup loop with larger area in the form of a magnetometer or a gradiometer connected to the on-chip integrated multi-turn input coil which is magnetically tightly coupled to the SQUID. The noise energy coupled to the SQUID is minimum only when $L_i = L_p$, where L_i and L_p are the inductances of the input coil and the pickup loop respectively. For a typical low- T_c dc SQUID and radius of the pickup loop $r_p \sim 10 \text{ mm}$, one can expect the white magnetic field noise of the order of $1 \text{ fT}/\sqrt{\text{Hz}}$. Such sensitivities can only be utilized fully inside a superconducting shield or in a magnetically shielded room. In unshielded environments, fluctuations in the earth's magnetic field, local fields at power line frequency and disturbances due to strong sources such as rotating machinery will dominate the applied magnetic field to the SQUID. For sensitive measurements using SQUID sensors, like the measurement of biomagnetic fields and high resolution measurement of magnetic susceptibility, the use of gradiometers for rejection of distant sources of magnetic noise is almost inevitable. Fig.5(b) shows the principle of a first derivative, axial gradiometer consisting of two pickup loops of equal turns areas connected in series; the two loops are wound in opposition and are separated by the baseline, b . A uniform magnetic field B_z ideally induces zero net screening current into the two loops, and hence couples no net flux to the SQUID. A gradient $\partial B_z/\partial z$, on the other hand, induces a net screening current in the gradiometer, which flows through the input coil and a corresponding flux is inductively coupled to the SQUID. Fig.5(c) shows the configuration of the second derivative axial gradiometer consisting of two first derivative gradiometers wound in opposition. For uniform magnetic field and first order field

gradient, the net screening current induced in the second order gradiometer is zero. The second derivative of the magnetic field $\partial^2 B_z / \partial z^2$ induces screening current in such a gradiometer and couples a net flux to the SQUID.

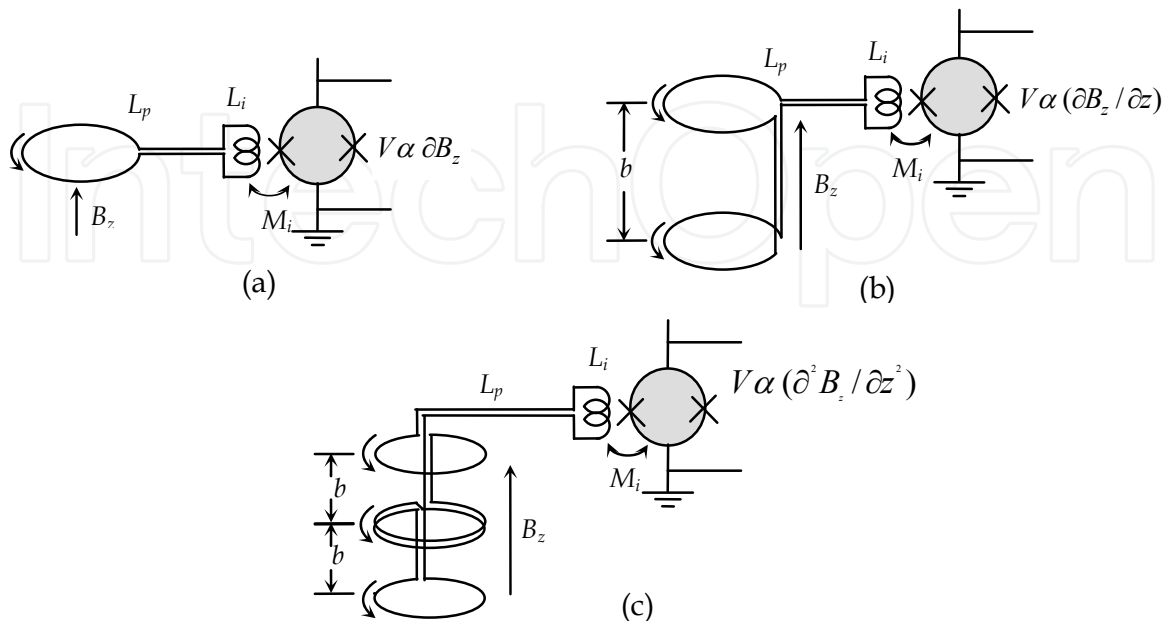


Fig. 5. Pickup loop configuration with different geometries connected to the input coil of the SQUID (a) magnetometer, (b) first order gradiometer and (c) second order gradiometer

The SQUID based measuring system has to be designed based on the nature of the signal source of interest. In some cases the signal source may be exposed to high temperature, high magnetic fields like magnetization measurements and in some other cases like nondestructive testing, biomagnetism, geophysics, SQUID microscope etc. the signal source may have to be kept at room temperature and is often outside the cryostat.

5. SQUID based NDE system

The SQUID based NDE system designed and constructed in our laboratory consists of a SQUID probe with superconducting pickup loop in the form of first order axial gradiometer housed in a nonmagnetic liquid helium cryostat, stepper motor driven precision XY scanner with non-magnetic platform for the sample movement and the data acquisition module to acquire the SQUID output signal with respect to the positional coordinates of the sample which is under investigation.

5.1 SQUID probe

The SQUID probe comprises of a SQUID sensor and a superconducting first order gradiometer connected to the input coil of the SQUID. The SQUID sensor is enclosed by a superconducting magnetic shield while the superconducting gradiometer is exposed to detect the magnetic signal of interest. The local source of interest generates a much larger field gradient at detector (superconducting pickup loop) than that generated by a more distant noise source.

A holder to mount the SQUID sensor together with a former to wind the pickup loop of the gradiometer has been fabricated as a single piece and is connected at one end of the 13 mm diameter thin walled stainless steel (SS) tube designed to be insertible in a liquid helium cryostat. The electrical leads in the form of twisted pairs as required for the SQUID sensor are routed through the thin walled SS tube and terminated at the top with appropriate electrical feedthroughs. A first order gradiometer made of superconducting NbTi wire with diameter of 0.1 mm is wound over the former and is inductively coupled to the SQUID device. The gradiometer consists of two loops of 4-mm diameter wound in opposition and separated by a baseline of 40 mm. This configuration enables discrimination against distant sources of magnetic noise which produce equal and opposite response from the two loops constituting the gradiometer. The SQUID sensor is shielded with a lead cylinder with an inner diameter of 16 mm and a length of about 120 mm.

The SQUID probe is housed in a FRP liquid helium cryostat having a capacity of 11.5 litres of liquid helium. The cryostat has a low boil-off rate of under 2.2 litres per day and is designed to have a minimum warm-to-cold distance of 6 mm. The cryostat is equipped with a top loading clear access of 25 mm diameter for the insertion of SQUID probe. The cryostat was constructed with fiberglass-reinforced epoxy, which has been found to have suitable structural and thermal properties without introducing a high level of magnetic noise and distorting noise fields. The setup was calibrated by measuring the system response to the magnetic field produced by a large circular coil and the calibration constant was inferred to be 20 nT/cm per flux quantum coupled to the SQUID. Fig.6. shows the cross sectional view of the SQUID probe housed in a liquid helium cryostat.

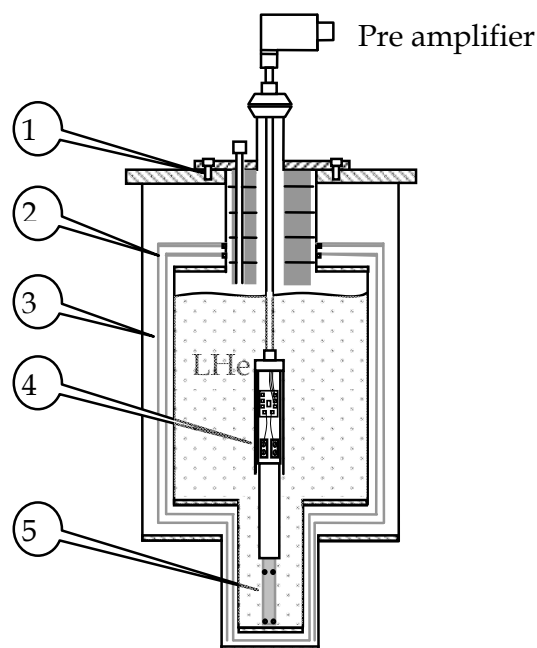


Fig. 6. Cross sectional view of the SQUID probe housed in liquid helium cryostat. 1. LHe cryostat, 2. Radiation shields, 3. Vacuum space, 4. SQUID, 5. Pickup loop

5.2 XY scanner

One of the most important requirements for SQUID based NDE system is the scanner to move the specimen in order to scan it under the stationary liquid helium cryostat. In most SQUID based NDE systems, the specimen is moved under a rigidly fixed stationary SQUID system. Commercial general purpose scanners are not suitable for the SQUID NDE applications because of the use of magnetic materials in their construction and the consequent generation of heavy electromagnetic noise. Therefore a stepper motor driven nonmagnetic precision XY scanner has been specially designed and fabricated for SQUID NDE system operating in our laboratory to enable precision movement of the sample.

The XY scanner has been designed for the scanning of flat plate samples with a positional accuracy of 0.025 mm and repeatability of 0.1 mm. The detailed specifications of the XY scanner have been listed in Table 2. The major components of the XY scanner are computer controlled XY stage, supporting platform which moves smoothly over a frictionless table and a non-metallic and non-magnetic sample holder. The whole assembly has been mounted on a single frame. Necessary vibration isolation has been provided to minimize the transmission of floor vibrations. Care has been taken to isolate the SQUID system from the magnetic noise generated by the high torque stepper motors. The details of the XY scanner are discussed below.

Sample	Flat plates
Scanning area	300 mm x 300 mm
Step size	0.25 mm to 5 mm
Speed	1 to 50 mm/sec

Table 2. Specifications of X-Y scanner

5.2.1 XY scanner: Computer controlled XY stage

The main component of the XY scanner is a computer controlled stepper motor driven XY stage. For flat samples the XY table is activated to scan the sample in either X or Y directions. The XY table has a traverse of 300 mm in each direction and is driven by two stepper motors (model KML092F13, Warner SLOSYN). Each stepper motor is connected to a micro-stepping driver (SS2000 MD808, Warner SLO-SYN) controlled by a programmable stepper motor controller (model SS2000PCi, SLO-SYN). The motion is achieved by driving the lead screws through the stepper motors to achieve the desired position of the table. Each axis of the stage is equipped with proximity switches which set the travel end-limits of the stage and also define the home position. The home position is a reference point from which all distances are measured, and is always approached from the positive end of travel limit with a preset velocity and acceleration, to ensure the reproducibility of scans to better than 0.1 mm. In addition, there are safety limit switches at both ends for over travel protection.

5.2.2 Supporting platform

Since the SQUID system is extremely sensitive to any magnetic flux changes, it is necessary to keep this system far away from the stepper motors. The high frequency current pulses applied to the high torque stepper motors generate undesirable magnetic field noise, which could disturb the locking of the sensitive SQUID system. To avoid such magnetic noise, the

stepper motors have been located 2.5 m away from the SQUID system. The sample holder has been mounted at one end of the supporting platform which is made of non-magnetic and non-metallic materials. Since the platform has a large length, two pairs of roller tables have been provided. The central one is made of a stainless steel case with brass ball bearings and the other one close to the sample holder is made of a nylon case with glass ball bearings. These rollers smoothly move over the frictionless tables. The supporting frame is made of fiber glass square pipes. The fasteners used in the region close to the sample holder are made of nylon.

5.2.3 Sample holder

The sample holder is fabricated using non-metallic and non-magnetic materials such as fiberglass and polypropylene. Care has been taken to avoid the use of any magnetic components around the sample holder up to a radial distance of about 500 mm.

5.2.4 Shielding

Even though the stepper motors are kept far away from the SQUID system, it was found that the SQUID picks the magnetic field noise associated with the stepper motors causing the SQUID system to frequently unlock. The noise level has been reduced to some extent by covering the stepper motors by two layers of μ - metal and by wrapping all the cables coming from the control panel to XY stage by a flat copper braid. The flat copper braid has been properly grounded with the main power ground. The electrical leads coming from the SQUID to the preamplifier mounted at the top of the liquid helium cryostat and the leads that connect the preamplifier to the flux locked loop electronics module kept in the instrument rack have also been shielded and the shield is properly grounded.

5.3 Data acquisition system

Fig.7 shows the schematic diagram of the SQUID based NDE measurement system. The specimen or the source of magnetic signal is mounted over the sample holder of the XY scanner. Whenever there is a change of magnetic flux in the vicinity of the pick-up loop, a screening current is induced in the pickup loop, which is inductively coupled to the SQUID. The SQUID in conjunction with the flux locked loop readout electronics generates a voltage output which is proportional to the magnetic field gradient, $(\partial B_z / \partial z)$ over the baseline of the pick-up loop. The oscilloscope is used to display the necessary signals for tuning the SQUID readout electronics by setting optimum bias current, amplitude of modulation flux, etc. A complete data acquisition system has been developed based on Visual Basic. The user can select the initial and the final positions of the sample coordinates, step size and scanning speed for each scan axis. The software selects grid points within the selected area depending upon the specified step size. The sample is scanned under the SQUID system and the SQUID output is recorded in the computer as a function of position coordinates. For every specified step size, the intelligent micro-stepping drive unit sends TTL pulse to the data logger (model 34970A, Agilent), which stores the data in its buffer whenever a trigger pulse is received from the drive unit; the first data is collected by a software trigger. After each line scan (say y-axis) the sample is moved one step with the specified step size perpendicular to y-axis (say x-axis). During this time the data is transferred from the data

logger to the computer and stored for further analysis. This wait time is user selectable before the start of scan. In addition to this, a linear scale has been provided along each scan axis and the actual position coordinates displayed in a digital readout. Provision has been made for manual operation of each scan axis, and for selection of home position for each scan axis. Fig.8 shows the photograph of the SQUID based NDE system with XY scanner.

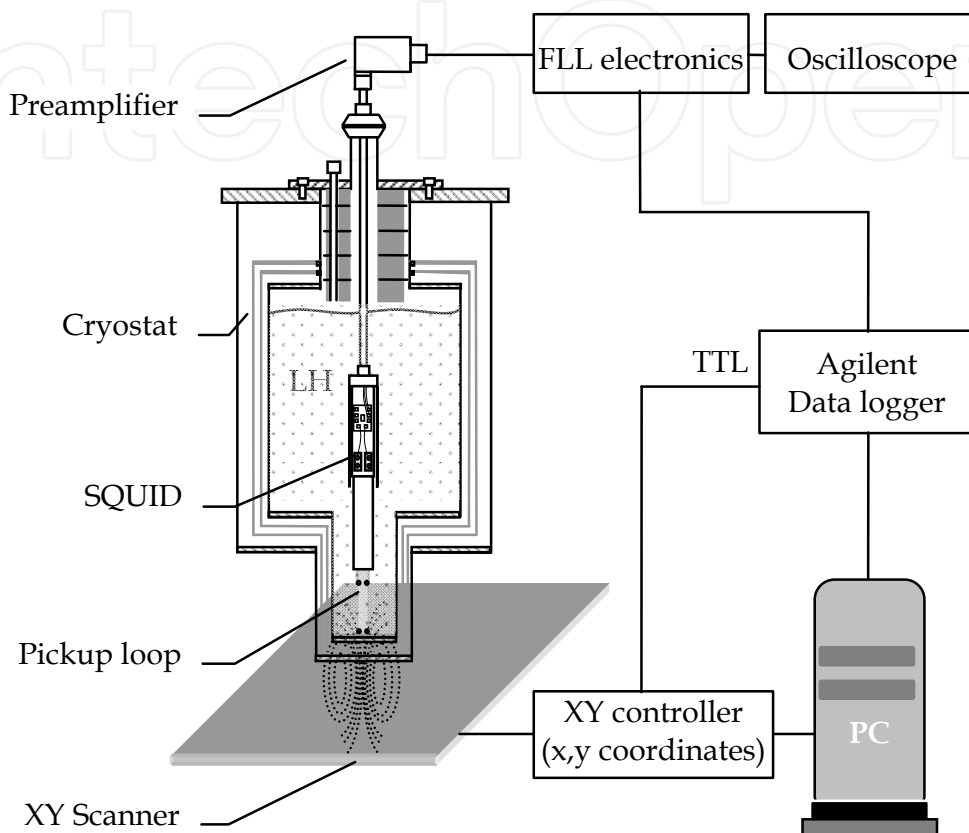


Fig. 7. Block diagram of the SQUID based NDE system



Fig. 8. Photograph of the SQUID based NDE system

To check the performance of the system a steel ball weighing 2.2 mg has been magnetized by applying a magnetic field of about 35 Oe for a preset time of about 5 minutes. The magnetized steel ball has been scanned under the SQUID system to measure the remanent magnetization. After scanning, the steel ball has been removed and the background noise has been recorded. It may be noted that even though the sample platform is made of non-magnetic material, the Y table which moves over the X table in the XY scanner is constructed by using lead screws and linear guides which are magnetic. The contribution of the background has been eliminated by subtracting the background from the signal. Fig 9 shows the recorded SQUID output voltage for the magnetized steel ball while it is scanned under the SQUID system. The amplitude of the magnetic anomaly associated with the 2.2 mg steel ball is about 80 millivolts while the width of the magnetic anomaly arises on account of the stand-off distance of about 10 mm between the steel ball and the sensing loop. It may also be noted that based on the noise floor, one can estimate that the SQUID based NDE system can detect the presence of a steel particle weighing as low as 10 μ g at signal-to-noise ratio unity.

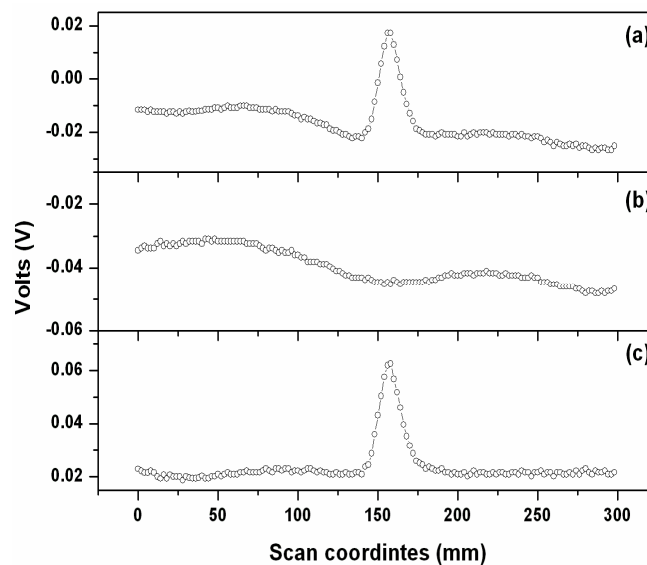


Fig. 9. Recorded SQUID output voltage for the steel ball scanning under the SQUID. (a) Steel ball with background noise (b) background noise and (c) steel ball alone

6. Utilization of SQUID based NDE system

This SQUID system has been used for the measurement of subsurface defects by inducing eddy currents in conducting materials at relatively low frequencies and also for the measurement of extremely low content of δ -ferrite in the 316L(N) stainless steel weldment specimens which are subjected to low cycle fatigue at high temperatures.

6.1 SQUID based eddy current NDE

Conventional eddy current testing is the popular NDE technique for detecting subsurface defects in conducting structures like aluminum, stainless steel etc. In this technique, eddy currents are excited in a conductor using a magnetic field varying in time at an excitation frequency f .

A suitable coil carrying AC current is used to induce eddy currents in the specimen by producing a time varying magnetic field. The physical basis for the eddy current induction in conducting material is contained in the Faraday's law $\nabla \times \vec{E} = -\frac{\partial \vec{B}}{\partial t}$ which can be rewritten as

$$\nabla \times \vec{J} = -\mu\sigma \frac{\partial \vec{H}}{\partial t} \quad (3)$$

where μ is the magnetic permeability and σ is the electrical conductivity of the material. The time varying applied magnetic field will induce a current distribution inside the conductor in accordance with equation 3 and these currents are referred to as eddy currents.

If the applied magnetic field varies sinusoidally with respect to time, $H = H_0 e^{i\omega t}$, then eq. (1) becomes

$$\nabla \times J = -i\omega\sigma\mu H \quad (4)$$

In qualitative terms, the curl of the eddy currents is out of phase with the applied time varying magnetic field, is proportional to the frequency of the applied magnetic field and opposes the changes in the applied magnetic field with time. In conventional eddy current NDE, sinusoidal current with the frequency ranging from 10 kHz to 10 MHz is passed through an excitation coil having hundreds of turns and the voltage induced across the coil is measured to determine the impedance of the coil. The presence of a conductor near the coil affects its impedance and the changes in the coil impedance are measured which are associated with changes in some characteristics of the conductor (variation in local thickness, conductivity or permeability due to the presence of defects). In the case of SQUID based eddy current NDE the change of the magnetic field due to the presence of a defect is directly measured by the SQUID. The defects perturb the flow pattern of the induced eddy currents in the conductor and hence they manifest as localized magnetic anomalies when the conducting plate is scanned under the SQUID sensor. The amplitude and shape of the magnetic anomaly corresponding to a defect depend on the amplitude of the eddy current flowing in the immediate vicinity of the defect and also on the defect characteristics such as size, orientation etc. The use of higher excitation frequencies tends to increase the amplitude of the eddy currents induced on the surface; however, the strength of the eddy current induced exponentially decreases with depth d measured from the surface as $e^{-d/\delta}$, where δ is the skin depth defined as

$$\delta = \left(\frac{1}{\pi f \mu \sigma} \right)^{1/2} \quad (5)$$

Here f is the frequency of the excitation current used to induce eddy current in the conducting material. In the conventional eddy current testing, excitation frequencies higher than 10 kHz are generally used to increase the voltage induced in the pick-up loop; therefore, the depth of the defect detection is limited by the skin depth (δ) of the material, which is rather low at such high frequencies. If the excitation frequency is reduced in order

to increase the skin depth, the induced voltage in the pick-up loop also decreases, often reaching the system noise floor, and thus severely limiting the depth of defect detection. The system based on the use of SQUID as a detector promises better signal-to-noise ratio at lower operating frequencies. Since the sensitivity of the SQUID device is independent of the operating frequency from near dc to several kHz (white noise regime), it is possible to use a SQUID based system for the detection of deep subsurface defects, which are not detectable in the conventional eddy current testing owing to skin depth limitations. In the SQUID based system, pickup loop can be wound using superconducting wire; unlike normal metal pickup loops for which induced voltage is proportional to the rate of change of flux, superconducting pickup loop directly senses the change in magnetic flux and hence its use is crucial in retaining the requisite low frequency sensitivity. Several groups have successfully utilized this feature to detect subsurface defects not detectable by conventional eddy current techniques (W.G. Jenks et al., 1991; P. Chen et al., 2002; H. Weinstock, 1991; M. Mück et al., 2005; U. Klein et al., 1997).

The excitation coil used to induce eddy currents in the SQUID based eddy current NDE is also often different from that used in the conventional eddy current methods. In conventional testing, the excitation coil is in the form circular coil and in some cases a set of differential coils are used. To enhance the eddy current in the specimen, it is required to apply a large time varying magnetic field. If we use circular excitation coil for the SQUID based eddy current NDE system the direct magnetic field coupled to the SQUID is very large and the output voltage of the flux locked loop readout electronics may reach saturation levels. Under these conditions, the changes of magnetic field due to the presence of a defect cannot be detected by the SQUID. To overcome this, a double "D" excitation coil at room temperature, placed just below the cryostat, is often used to excite eddy currents in the specimen at room temperature. This double "D" configuration for the excitation coil enables realization of a wide dynamic range since the direct coupling of magnetic flux to the pick-up loop is a minimum when the axis of the excitation coil coincides with that of the pick-up loop. The schematic view of the double "D" excitation coil and the location of the superconducting pick-up loop are shown in fig.10. The central axes of the excitation coil and the pick-up loop are adjusted to coincide and held stationary during the measurement. The current in the double "D" coil flows through the central straight segment and then around the perimeter of the semicircular loops. Thus the field through one D section of the coil is always 180 degrees out of phase with the field through the other D section of the coil. The specimen, which is to be evaluated, is kept at room temperature at a stand-off distance of about 14 mm from the bottom loop of the superconducting gradiometer located inside the cryostat and is scanned under the stationary liquid helium cryostat. Eddy currents were excited in the specimen under investigation using the double "D" coil with 120 turns and an overall diameter of 40 mm carrying a current of 150 mA(rms). Changes in the induced eddy current flow associated with the presence of a defect manifest as changes of the flux signal detected by the SQUID device as the specimen is scanned. The SQUID, in turn, produces an output voltage corresponding to these changes in magnetic flux. This output is phase sensitively detected by a lock-in-amplifier whose reference channel is fed by the oscillator, which is used to supply the necessary excitation current to the double-D coil. The schematic diagram of the experimental set-up for the SQUID based eddy current NDE is shown in fig.11.

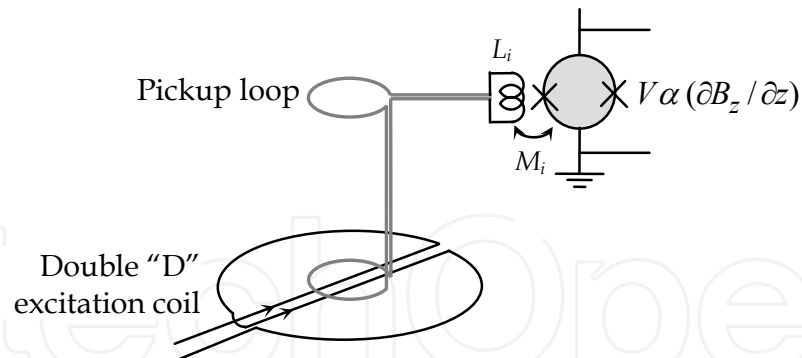


Fig. 10. Schematic view of the double "D" excitation coil and pickup loop arrangement

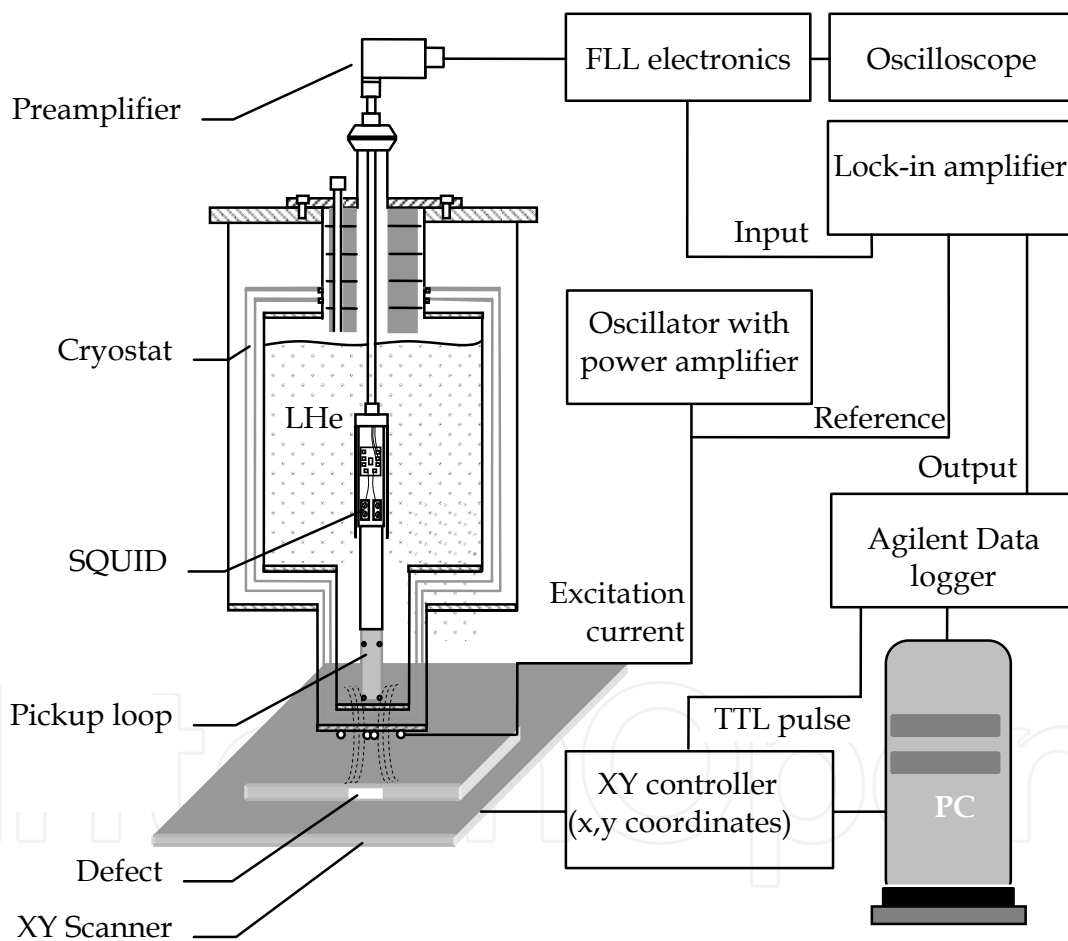


Fig. 11. The SQUID based eddy current NDE system

Both the real (in-phase with the excitation current) and imaginary (90° out-of-phase with the excitation current) components of the SQUID output voltage were measured using the lock-in-amplifier and were simultaneously recorded by a computer with respect to the positional coordinates of the defect as the plate was scanned under the stationary cryostat using a precision X-Y scanner.

6.2 Remnant magnetization measurements

Fatigue damage and effect of thermal ageing are the most important problems for a number of high temperature components in power plants particularly in welded regions. Austenitic stainless steels are the preferred materials for sodium cooled fast breeder reactors as they possess excellent high temperature mechanical properties for nuclear reactor service. A nitrogen-added low carbon version of SS 316 austenitic stainless steel (316 L(N)) has been chosen for the high temperature components of Prototype Fast Breeder Reactor (PFBR) in India. A major consideration during the welding of 316 L(N) stainless steel is its resistance to hot cracking. The presence of an optimum amount of delta ferrite in the austenitic weld metal is desirable to prevent hot cracking in the weldment. However the δ -ferrite structure is highly unstable during high temperature service and transforms to carbides and brittle intermetallic phases, e.g. sigma phase. Small quantities of these phases would cause large variations in the mechanical properties and influence corrosion behaviour of the material. Hence the knowledge of these phases such as type, amount etc is essential in designing the optimal operational parameters to achieve the desired lifetime for welded stainless steel components. Since the δ -ferrite is a magnetic phase, one can evaluate the δ -ferrite content by measuring remanent magnetization of the weldment sample. Since the SQUID device has an extremely high sensitivity for magnetic flux signals, one can detect an extremely low content of δ -ferrite in the weldment samples through remanent magnetization measurements. The experimental set up for the remanent magnetization measurements is similar to that shown in fig.11 except that the double "D" excitation coil is not used. In this case, the SQUID output is directly read by data logger and recorded by the computer with respect to the coordinates of the sample as it is scanned under the stationary cryostat.

7. Results of experimental investigations

We have carried out two different kinds of studies such as detection of artificially engineered subsurface flaws in aluminum plates by using the SQUID based eddy current technique and NDE of fatigue cycled stainless steel weldment specimens to detect the δ -ferrite content through remanent magnetization measurement by the SQUID system.

7.1 Detection of subsurface flaws in aluminum plates

The SQUID based NDE system has been initially tested with an aluminum plate with a length of 300 mm, width of 100 mm, and thickness of 10 mm with artificially engineered defects, as shown in fig. 12 (a). Two rectangular defects have been engineered with a separation of 150 mm. One defect has a length of 50 mm, width of 1 mm, and height of 1 mm, and another defect has a length of 50 mm, width of 1 mm, and height of 0.5 mm and the magnetic anomalies corresponding to these two defects were studied as part of initial exploratory studies on subsurface defect characterization. Eddy currents were excited at a relatively low frequency of about 200 Hz using double "D" excitation coil. The aluminum plate with defects on its bottom surface was scanned under the SQUID probe and the changes of magnetic field associated with the defects were recorded with respect to the positional coordinates. Fig. 12 (b) shows the magnetic anomalies associated with these defects recorded using a SQUID. The amplitude of the magnetic anomaly corresponding to a defect having a height of 1 mm was 2.3 nT/cm. Since the noise floor of the system is few

tens of pT/cm, it is estimated that even a localized loss of conductor thickness as low as 0.1 mm can be detected at a depth of 9 mm at signal to noise ratio unity. The potential of the system for detection of subsurface defects using low-frequency eddy current excitation is evident from this data.

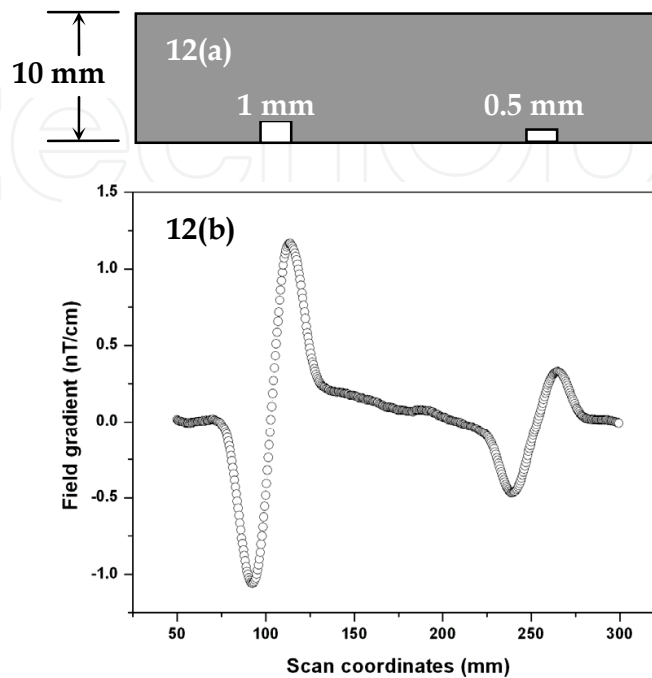


Fig. 12. (a) Aluminum plate with artificially engineered defects. (b) Magnetic anomalies associated with the defects buried at a depth of 9 mm below the surface recorded by the SQUID.

Subsequently detailed experimental studies have been carried out for the determination of optimum eddy current excitation frequencies for the defects located at different depths below the top surface of an aluminum plate. This optimum excitation frequency corresponds to the frequency at which the amplitude of the magnetic anomaly associated with a defect at a certain depth reaches a maximum value. The optimum excitation frequency has been theoretically investigated by Sikora et al (R. Sikora et al., 2003) and by Baskaran and Janawadkar (R.Baskaran and M.P. Janawadkar, 2004) using the analytical solution (C.V.Dodd & W.E. Deeds, 1968) to the distribution of eddy currents excited by a circular coil in a defect free semi-infinite conductor. It may, however, be noted that the results of these theoretical investigations cannot be directly compared with the experimental results reported here since in the present studies, a non-axisymmetric double-D coil was used as an excitation coil to induce eddy currents in a conductor stack of finite thickness with a defect embedded within the stack.

A set of aluminum plates with a length of 300 mm, width of 200 mm and with different thicknesses ranging between 2mm to 12 mm in steps of 2 mm were fabricated for this study. An artificial defect is engineered in a separate 1 mm thick aluminum plate with a defect length of 60 mm and width of 0.75 mm to simulate a localized loss of conductor volume in the plate. The length and width of the plate carrying the defect are identical to those of the plates without defects. SQUID based eddy current NDE measurements have been carried

out for the stack of aluminum plates with the defect plate located at different depths ranging from 2 mm to 14 mm (in steps of 2 mm) while keeping the total thickness of the conductor stack to have a constant value of 15 mm throughout the experimental investigations. As an example, to simulate the defect located at a depth of 2 mm below the top surface, the defect plate was sandwiched between a 2 mm thick aluminum plate at the top and a 12 mm thick aluminum plate at the bottom. An interchange of the top and bottom plates shifts the defect location to 12 mm below the top surface. In this way, the location of the defect was shifted to different depths from 2 mm to 14 mm below the surface. A photograph of the aluminum plates used in this study in order to vary the defect depth is shown in fig. 13. The stack of plates was scanned under the SQUID in a direction such that the defect length is perpendicular to the scanning direction. To avoid edge effects, the scanning region was limited to a total length of 120 mm (60 mm on each side of the defect). For each scan, both the real and imaginary components of the SQUID output voltage were measured using the lock-in-amplifier and were recorded with respect to the positional coordinates of the defect. For each defect depth, the experiments were repeated at different excitation frequencies ranging between 33Hz and 853Hz in steps of 20 Hz.

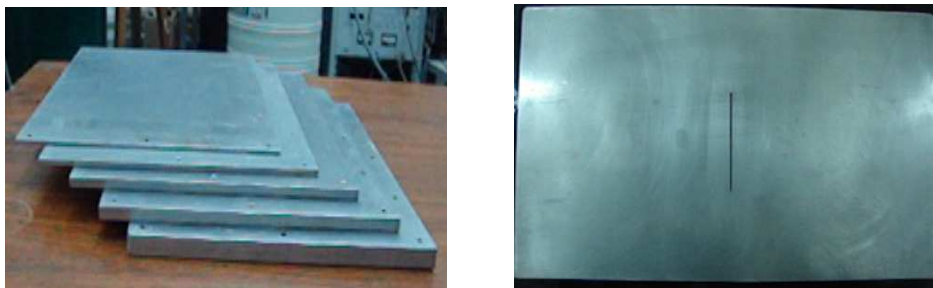


Fig. 13. Aluminum plates used in the study (plate with the defect is also shown).

As an illustration of the magnetic anomaly detected by the SQUID system, fig. 14 shows the measurements corresponding to defect located at a depth of 14 mm below the top surface when the eddy currents are excited at the frequency of 33 Hz, 103 Hz and 243 Hz. At the lower excitation frequency of 33 Hz, the skin depth is high and the resultant amplitude of the change of magnetic field gradient due to the defect is 0.657 nT/cm. At the higher excitation frequency of 103 Hz, the skin depth is lower but the induced eddy current amplitude is higher and thus the detected magnetic anomaly has a higher amplitude of 1.8 nT/cm. When the excitation frequency is further increased to 243 Hz, the exponential attenuation of the eddy current amplitude at the location of the defect more than compensates for the small linear increase resulting from the use of higher frequency of excitation; the amplitude of the detected magnetic anomaly therefore decreases to 1.356 nT/cm. In this case, as shown in fig.14 (b) one can also clearly see the signal changes due to the small variations in lift-off as the sample moves relative to the gradiometric pickup loop. At the optimum excitation frequency of 103 Hz, the signal to noise ratio is evidently better. It may also be noted that the phase of the magnetic anomaly changes systematically when the excitation frequency is varied as shown in fig.14. The change in the resultant amplitude of the magnetic anomaly corresponding to a defect located at a depth of 14 mm below the surface when eddy currents are excited at different frequencies is shown in fig.14(d). At low frequencies, the eddy current induced in the conductor stack has low amplitude and hence the amplitude of the magnetic anomaly associated with the defect is also low. As the

excitation frequency increases, the amplitude of the eddy current induced on the surface increases monotonically; however, owing to the skin effect, the amplitude of the eddy currents at a depth of 14 mm increases initially, reaches a maximum at the optimum excitation frequency of 103 Hz and decreases steadily thereafter. At higher frequencies, the eddy current tends to be concentrated at the upper surface of the material due to the skin effect. Therefore the amplitude of the magnetic anomaly due to the presence of the defect at a depth of 14 mm decreases when excitation frequencies higher than 103 Hz are used. In the present experimental investigations, the excitation frequency was varied from 33 Hz to 253 Hz in steps of 10 Hz and the optimum frequency was determined to be 103 Hz for the defect located at a depth of 14 mm below the surface. The experiments were repeated for defects located at different depths of 12 mm, 10 mm, 8 mm, 6 mm, 4 mm and 2 mm from the top surface and a comprehensive characterization of the magnetic anomalies was carried out as a function of defect depth and frequency. Fig.15 shows the magnetic anomaly detected by the SQUID system as the sample with defect located 10 mm below the surface is scanned. These plots show the variations in the magnetic anomalies resulting from the use of different excitation frequencies on the same scale. Fig. 16 shows the changes in the resultant amplitudes of the magnetic anomalies corresponding to defects located at different depths from the surface when eddy currents are excited at different frequencies. The excitation frequencies were varied in steps of 10 Hz for the defects at greater depths and 20 Hz for the defects at lower depths. The experimental parameters such as standoff distance, excitation

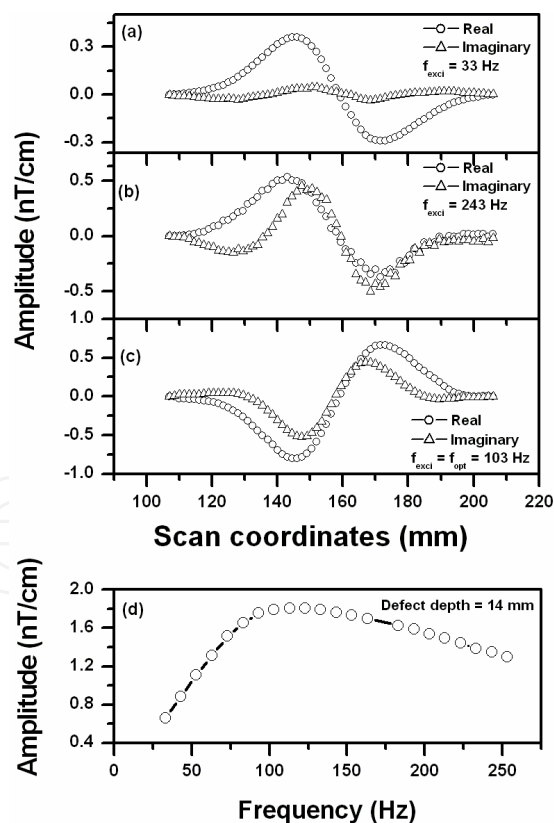


Fig. 14. (a),(b) and (c) show the changes in the magnetic anomaly corresponding to the defect buried at a depth of 14 mm below the surface with eddy current excitation at a frequency of 33 Hz, 243Hz and 103 Hz respectively. (d) The resultant amplitude of the magnetic anomaly due to the defect at different excitation frequencies.

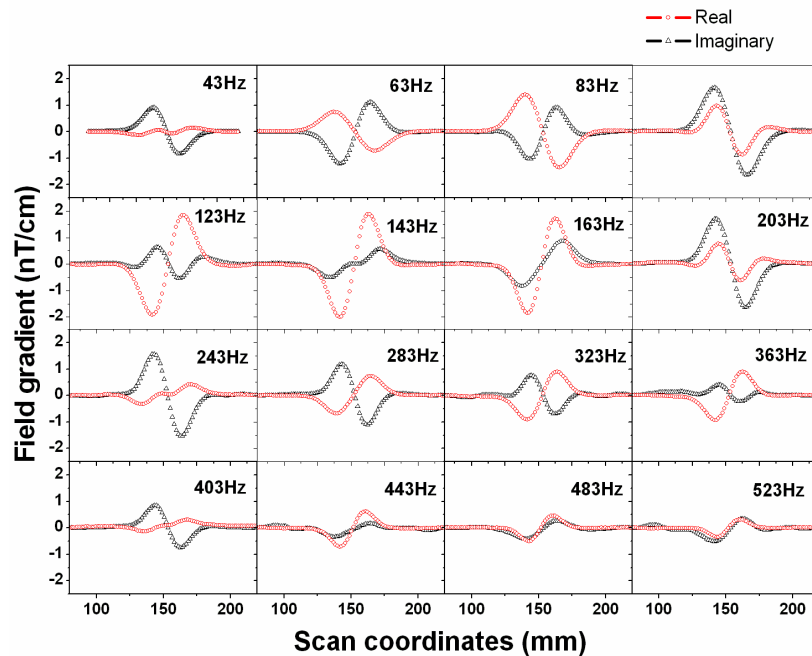


Fig. 15. The magnetic anomalies detected by the SQUID system for different frequencies when the defect was located 10 mm below the surface.

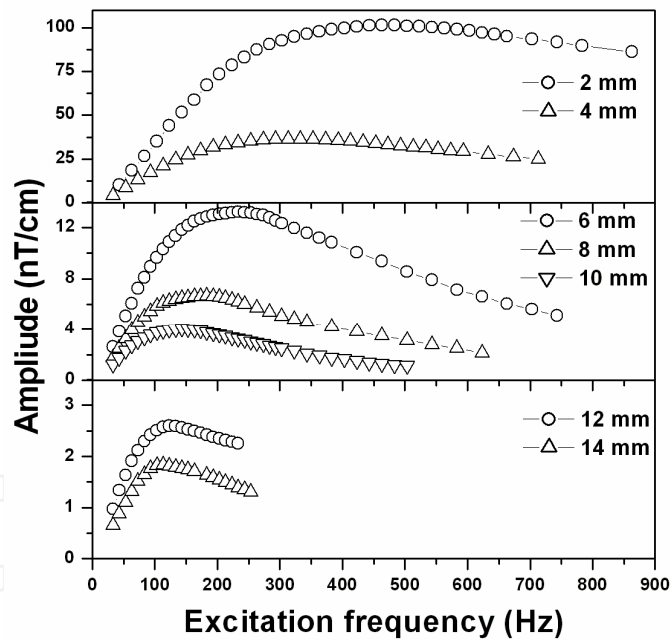


Fig. 16. The resultant amplitude of the magnetic anomalies corresponding to defects located at different depths when excited at different frequencies

coil current, flux locked loop electronics gain, scanning speed, step size, time constant of the lock in amplifier etc were kept constant for the entire series of experiments. The frequency at which the amplitude of the measured magnetic anomaly reaches a maximum value is taken to be the optimum frequency of excitation for defect located at a particular depth. As a result of these detailed experimental investigations, the optimum excitation frequencies have been estimated for the defects located at different depths from the surface and are listed in table 3.

Depth (mm)	2	4	6	8	10	12	14
f_{opt} (Hz)	453	313	233	183	143	123	103

Table 3. Optimum excitation frequencies for the defect at different depths

As shown in fig.17, the square root of the optimum excitation frequency is found to be inversely proportional to the defect depth. For the defects at lower depths from the surface, the signal to noise ratio is excellent for a wide range of frequencies; for the defects at greater depths from the surface, however, the range of frequencies which can be used for defect detection becomes narrow due to the poor signal to noise ratio and the skin effect of the conducting materials. It may also be noted that such defects can be detected only by using the SQUID based system for nondestructive evaluation.

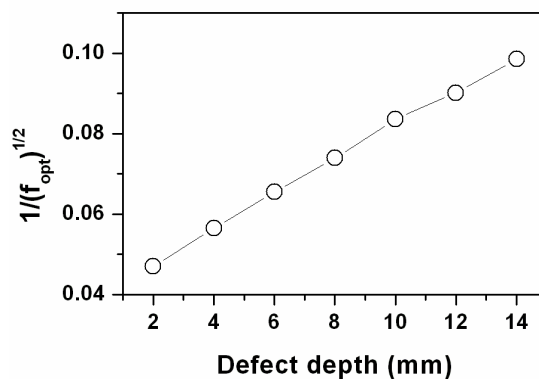


Fig. 17. The variation of the optimum excitation frequency with defect depth

7.2 Remanent magnetization measurements on fatigue cycled stainless steel weldments

The 316L(N) stainless steel weldment specimens were prepared by welding 316L(N) base metal with 316N electrodes by a manual metal-arc welding process. Welding was carried out on a 25 mm thick plate with a double-V configuration with an included angle of 70° (Fig. 18). Welds were radio-graphed and only sound joints were taken for the fabrication of the specimens. The low cycle fatigue (LCF) tests were conducted at a strain amplitude of $\pm 0.6\%$ using an Instron servohydraulic fatigue testing machine under total axial strain control mode at 600 °C. A strain rate of $3 \times 10^{-3} \text{s}^{-1}$ was employed for the test. The magnetic flux signal arising from the remanent magnetization of the sample was coupled to the SQUID device via a superconducting flux-transformer. As the sample was scanned under the cryostat, SQUID output revealed a characteristic magnetic anomaly when the center of the gauge length of the sample passed under the pickup loop indicating the presence of a magnetic phase at the location of the weld. To show the repeatability of the XY scanner a virgin weldment sample was scanned under the SQUID system for measuring the remanent magnetization. The sample was placed at room temperature; about 25 mm below the pickup loop and scanned using the XY scanner. The scanning started far away from the sample and as the sample approaches the pick up loop, SQUID output increased and it subsequently decreased as the sample moved away from the pick up loop. The experiment has also been repeated by rotating the sample by 90°, 180° and 270° about its central axis. As the sample was rotated about its axis, depending on the orientation of the magnetization of the sample

relative to the axis of the pick-up loop, the shape of the magnetic anomaly changed from bell shaped to dipolar. The magnetic flux profile measured near the center of the weldment sample for different angles of rotation is shown in Fig. 19. It may be noted that the center of the measured magnetic anomaly coincides for all scans showing excellent repeatability of the XY scanner. To show the system capability in measuring the virgin sample which was strongly magnetic and fractured sample which was magnetically very weak, the two samples were kept at a separation of 150 mm and scanned under the SQUID. Fig. 20 shows the magnetic flux profile for the virgin and the fatigue fractured sample. For the virgin sample, the amplitude of the magnetic anomaly was measured to be $\sim 1.78 \Phi_0$, whereas for the sample which was subjected to fatigue testing at 600 °C until fracture, the amplitude of the magnetic anomaly was measured to be as small as $\sim 0.05 \Phi_0$ under identical measurement conditions. To complete the SQUID based measurements, measurement of δ -ferrite was also carried out using a magnagage along the 25 mm gauge length of both the virgin and LCF tested samples. Figs. 21 (a) and (b) show the δ -ferrite distribution profiles in the virgin and LCF tested specimens respectively. Measurements were made in two

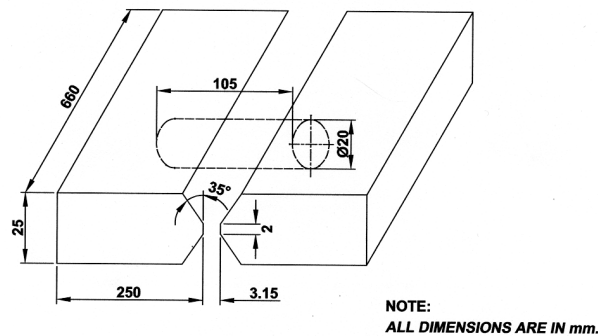


Fig. 18. Weld pad geometry used for the weld joint specimens.

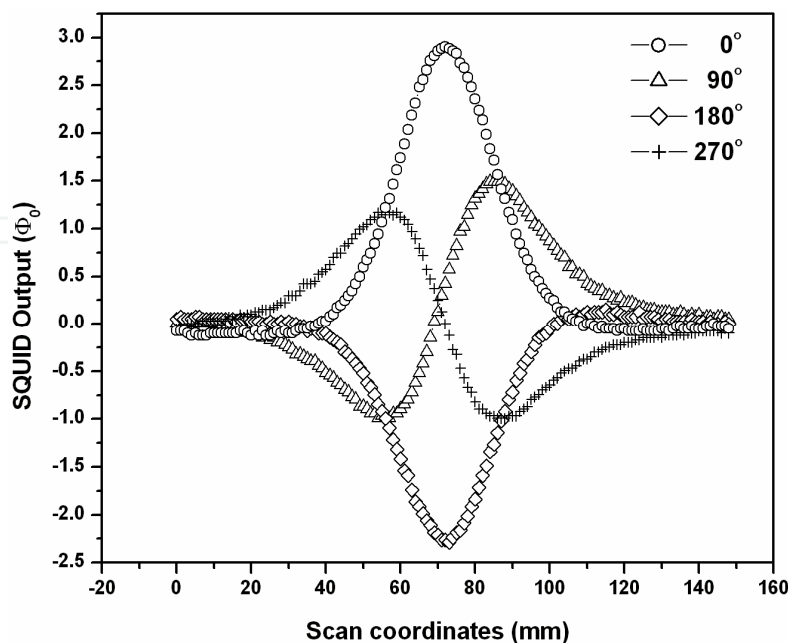


Fig. 19. Magnetic line profiles perpendicular to the gauge length of the weldment samples for different angles of rotation.

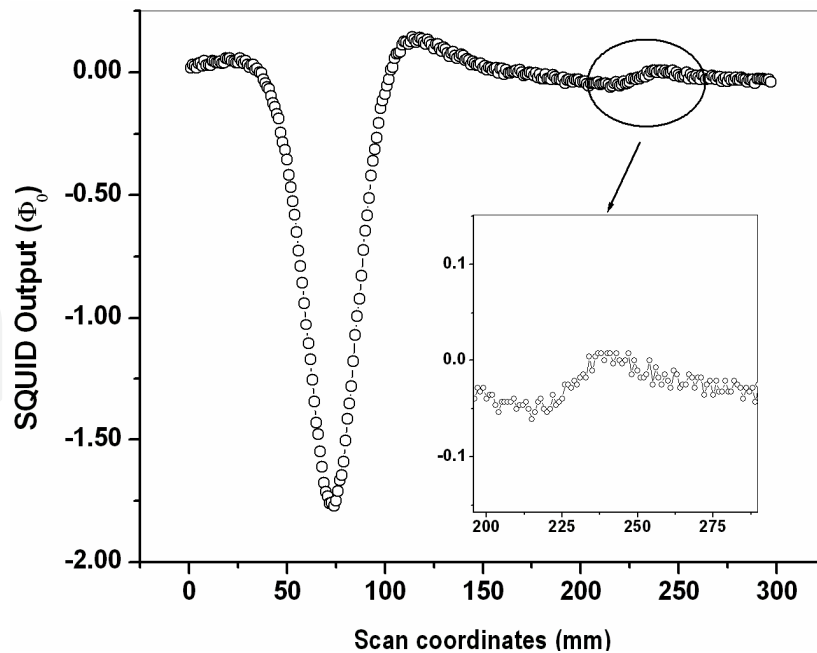


Fig. 20. Comparison of the magnetic flux profiles for the virgin and the fractured samples.

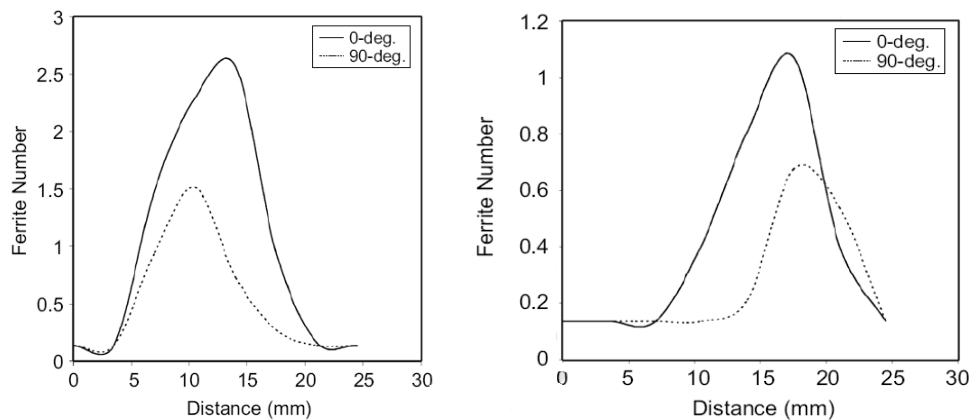


Fig. 21. (a) Delta ferrite distribution profile in the virgin sample. (b) Delta ferrite distribution profile in the LCF tested sample.

different orientations 90° apart from the central axis. The δ - ferrite was seen to peak around the mid-gage portion consisting of the joint proper. A considerable reduction in the amount of δ - ferrite after the LCF cycling could be seen. The experiments clearly show that the magnetic phase present in the virgin samples transforms to a non-magnetic phase (σ or carbides, etc.) during the fatigue deformation at 600°C . The transformation of δ - ferrite to brittle σ - phase has been known to influence the cracking behavior and thereby the fatigue life in the weld metals and weld joints of 316 and 316 L(N) stainless steels (M.Valsan et al., 1995, 2002; A. Nagesha et al., 1999). The amount of transformation of the δ - ferrite into brittle phases has also been found to be a strong function of the temperature and frequency of testing (A. Nagesha et al., 1999). The results reported here demonstrate the potential of SQUID based measurements in tracking the magnetic-nonmagnetic (ex. δ - σ) transformation in stainless steel welds when subjected to high temperature fatigue loading. A series of experiments has been carried out in the stainless steel weldment specimens to evaluate the

transformation of magnetic phase to nonmagnetic phases at different levels of fatigue deformation. In this study, a single weld joint was selected for remanent magnetization measurements in the virgin state and subsequently after every 50 fatigue cycles. At every stage prior to fatigue cycling and remanent magnetization measurement, the weld joint was properly demagnetized by subjecting it to low-frequency alternating magnetic field to eliminate the influence of the past history and then remagnetized by applying a preset dc magnetizing field (35 Oe) for a preset time (300 s) before the measurement of remanent magnetization using the SQUID-based setup commenced. The peak value of demagnetization field was kept slightly higher than the magnetizing field. To evaluate the relative changes in the magnetic content of the weldment specimen, the parameters of the measurement setup such as stand-off distance, FLL gain, etc., were maintained constant throughout the whole series of measurements. The virgin weldment specimen gave a maximum SQUID signal of $15 \Phi_0$, which decreased rapidly to $6.67 \Phi_0$ when the sample was subjected to LCF for 50 cycles. Thereafter, no significant changes in the maximum SQUID signal could be observed up to 150 cycles. However, a marked decrease in the SQUID signal was noticed when the sample was subjected to LCF for 200 cycles accompanied by the initiation of a crack at the boundary of the weldment specimen. Micro cracks were seen at the boundary of the weldment specimen when the specimen was examined through a microscope. The magnetic profile of the weldment specimen scanned under the SQUID probe is shown in fig. 22 in the virgin state as well as after subjecting the specimen to different levels of fatigue deformation. Fig. 23 shows the variation in the maximum SQUID signal as a function of the number of cycles of fatigue loading and portrays the transformation of magnetic δ -ferrite to nonmagnetic phases when the weldment specimen is subjected to LCF at 600 °C. It may be noted that although the initial signals were large, SQUID-based measurements were intended to look for small magnetic anomalies, if any, which could be correlated with the residual life of the weldment specimen. Further experiments are underway to clarify these issues.

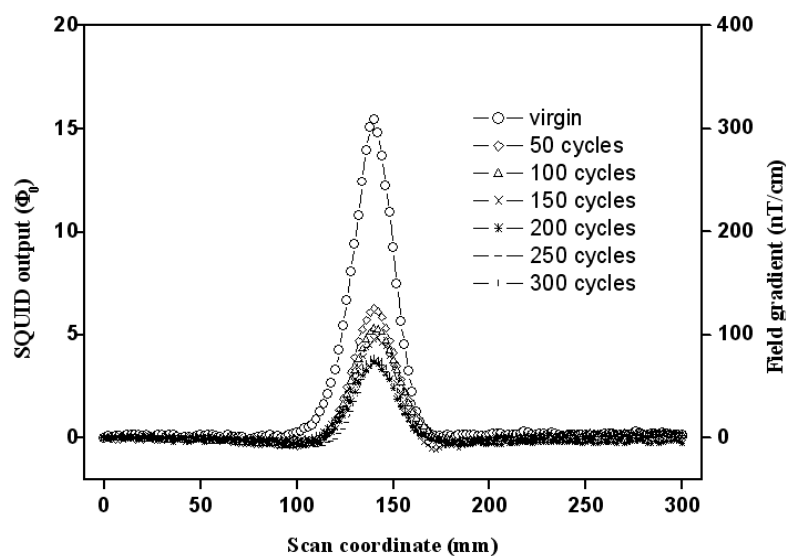


Fig. 22. Magnetic flux profile for the virgin and fatigue cycled weldment specimen

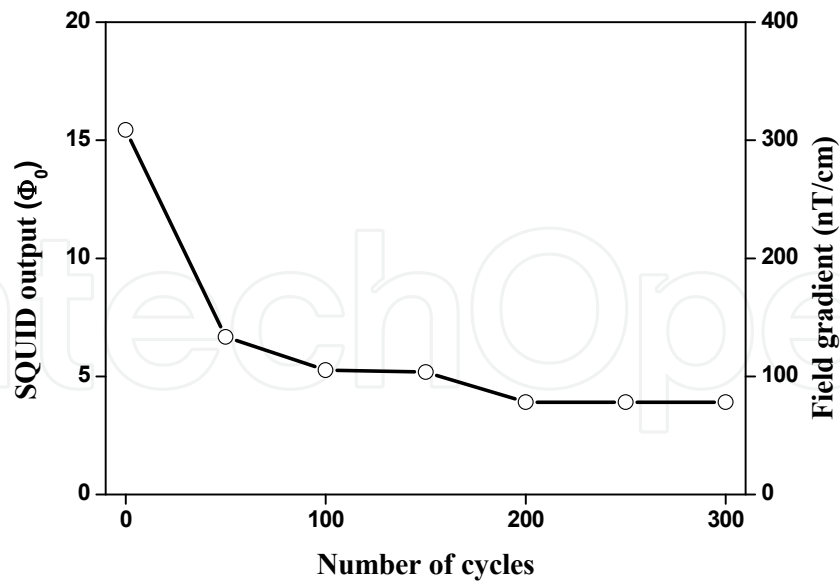


Fig. 23. Change of SQUID output vs number of fatigue cycles for the weldment specimen subjected to fatigue deformation

8. Conclusions

It is evident that the high magnetic field sensitivity of the SQUID sensors at relatively low frequencies can be usefully harnessed for a number of applications in nondestructive evaluation. In this chapter, we have attempted to illustrate the wide spectrum of possibilities by describing only a few representative studies and the reader is directed to the vast published literature in this emerging area. With the advent of HTS SQUID sensors operating at liquid nitrogen temperatures, SQUID based NDE is poised to be increasingly used in critical applications where the requirement of high sensitivity, not attainable by any other sensor technology, overrides the cost of cryogenic operating temperatures.

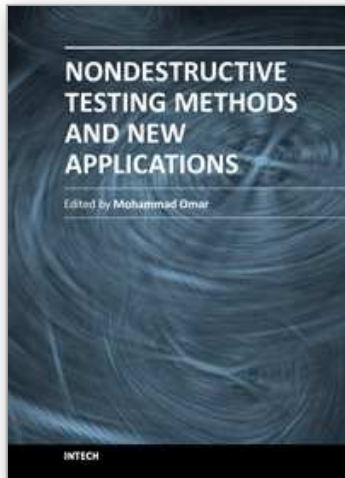
9. References

- Bain, R.J.P.; Donaldson, G.B.; Evanson, S. & Hayward, G. (1985) SQUID gradiometric detection of defects in ferromagnetic structures. In *SQUID '85 - Superconducting Quantum Interference Devices and their Applications*, (eds.) Hahlbohm, H.D. & Lübbig, H., pp. 841-846, ISBN 0899251447, Walter de Gruyter & Co., Berlin, New York
- Bain, R.J.P.; Donaldson, G.B.; Evanson, S. & Hayward, G. (1987). Design and operation of SQUID-based planar gradiometers for non-destructive testing of ferromagnetic plates. *IEEE Trans. Magn.* Vol. 23, No. 2, pp. 473-476, ISSN: 0018-9464
- Baskaran, R. & Janawadkar, M.P. (2004). Universal dependence of optimum frequency on defect depth for SQUID based eddy current evaluation. *Proc. National Seminar on NDE*, Pune, India, December 2004
- Chen,P.; Chen, L.; Li, J. & Ong, C.K. (2002). Novel excitation coils for non-destructive evaluation of non-magnetic metallic structures by high- T_c dc SQUID. *Superconductor Science and Technology*, Vol. 15, No.6, pp. 855-858, ISSN 0953-2048

- Clarke, J.; Goubau, W.M. & Ketchen, M.B. (1976). Tunnel junction d.c SQUIDs: fabrication, operation and performance. *J. Low Temp. Phys.*, Vol. 25, No. 1-2, pp. 99-144, ISSN 0022-2291
- Clarke, J. (1993). SQUIDs: theory and practice. in *The New Superconducting Electronics* (eds Weinstock, H. & Ralston, R. W., Kluwer, Dordrecht, pp.123-180, ISBN 0-7923-2515-X
- Dodd, C.V. & Deeds, W.E. (1968). Analytical Solutions to Eddy-Current Probe-Coil Problems, *J. App. Phys.*, Vol. 39, pp. 2829-2838, ISSN 0021-8979.
- Donaldson, G.B.; Cochran, A. & McKirdy, D.A. (1996) in: H. Weinstock (Ed.), SQUID sensors: Fundamentals, Fabrication and Applications, Kluwer, Dordrecht, pp. 599-628, ISBN 0-7923-4350-6
- Evanson, S.; Bain, R.J.P.; Donaldson, G.B.; Stirling, G. & Hayward, G. (1989) A comparison of the performance of planar and conventional second-order gradiometers coupled to a SQUID for the NDT of steel plates, *IEEE Trans. Magn.* Vol. 25, No. 2, pp. 1200-1203, ISSN: 0018-9464
- Hans Koch, H. (1989) in *Sensors - A Comprehensive Survey* (eds Boll, R. & Overshott, K. J.), VCH Publishers, NY, Vol. 5, pp. 381-445, ISBN 978-3-527-62058-6
- Jaycox, J. M. & Ketchen, M. B. (1981) Planar coupling scheme for ultra low noise DC SQUIDs *IEEE Trans. Magn.*, Vol. 17, pp. 401-403, ISSN 0018-9464
- Jenks, W.G.; Sadeghi, S.S.H. & Wikswo, J.P. (1997) SQUIDs for nondestructive evaluation. *J.Phys.D.* Vol. 30, pp. 293-323, ISSN: 0022-3727
- Klein, U.; Walker, M.E.; Carr, C.; McKirdy, D.M.; Pegrum, C.M.; Donaldson, G.B.; Cochran, A. & Nakane, H. (1997). Integrated low-temperature superconductor SQUID gradiometers for nondestructive evaluation. *IEEE Trans. Appl. Supercond.*, Vol. 7, No. 2, pp. 3037-3039, ISSN 1051-8223
- Krause, H.-J. & Kreuzbruck, M.v. (2002) Recent developments in SQUID NDE, *Physica C*, Vol. 368, No. 1, pp. 70 - 79, ISSN 0921-4534
- Krieger, J.; Krause, H.-J.; Gampe, U. & Sawade, G.(1999) . Magnetic field measurements on bridges and development of a mobile SQUID system. in: *Proc. Intl. Conf. on NDE Tech. Aging Infrastr.*, pp. 229-239, Newport Beach, USA, (March 1999)
- Lang, M.; Johnson, J.; Scriber, J.; Dobmann, G.; Bassler, H.J.; Eifler, D.; Ehrlich, R. & Gampe, U. (2000). Cyclic deformation behaviour of AISI 321 austenitic steel and its characterization by means of HTC-SQUID. *Nuclear Engineering and Design*, Vol. 198, No.1, pp. 185-191, ISSN 0029-5493
- Mück, M.; Korn, M.; Welzel, C.; Grawunder, S. & Schölz, F. (2005). Nondestructive evaluation of various materials using a SQUID-based eddy-current system. *IEEE Trans. Appl. Supercond.* Vol. 15, No. 2, pp. 733-736, ISSN 1051-8223
- Nagesha, A.; Valsan, M.; Bhanu Sankara Rao, K. & Mannan. S.L.(1999) Strain rate effect on the low cycle fatigue behaviour of type 316L(N) SS base metal and 316 SS weld metal, Proceedings of the international welding conference IWC'99, Vol. 2, February 15-17, 1999, New Delhi, pp. 696-703
- Sawade, G.; Straub, J.; Krause, H.J.; H. Bousack, Neudert, G. & Ehrlich, R. (1995). Signal analysis methods for remote magnetic examination of pre-stressed elements. in: Schckert, G. & Wiggerhauser, H. (eds) *Proc.Intl. Sympos.on NDT in Civil Eng. (NDT-CE)*, vol. II, DGZfP, Berlin, pp. 1077-1084

- Sikora, R.; Chady, T.; Gratkowski, S.; Komorowski, M. & Stawicki, K. (2003). Eddy Current Testing of Thick Aluminum Plates with Hidden Cracks. *Review of progress in Quantitative nondestructive evaluation*, Vol. 22, AIP Conference Proceedings, Vol. 657, pp. 427-434, ISBN 0-7354-0117-9, Bellingham, Washington, July 2002
- Tavrin, Y.; Siegel, M. & Hinken, J.-H. (1999). Standard method for detection of magnetic defects in aircraft engine discs using a HTS SQUID gradiometer. *IEEE Trans. Appl. Supercond.* Vol. 9, No.2, pp. 3809-3812, ISSN 1051-8223
- Valsan, M.; Sundararaman, D.; Bhanu Sankara Rao, K. & Mannan, S.L. (1995). High Temperature Low Cycle Fatigue of Steels and their Welds, *Metall. Mater. Trans.*, Vol. 26A, pp. 1207-1219, ISSN 1073 - 5623
- Valsan, M.; Nagesha, A.; Bhanu Sankara Rao, K. & Mannan, S.L. (2002). High temperature low cycle fatigue and creep-fatigue interaction behaviour of 316 and 316(N) weld metals and their weld joints. *Trans Ind Inst Met.* Vol. 55, No. 5 pp. 341-348, ISSN 0019-493X
- Weinstock, H. & Nisenoff, M. (1985) Nondestructive evaluation of metallic structures using a SQUID gradiometer, *SQUID '85, Proc. 3rd Int. Conf. On Superconducting Quantum Interference Devices and their Applications* (eds) Hahlbohm, H.D. & L'ubbig, H. (Berlin: deGruyter) pp. 843-847 ISBN 0899251447
- Weinstock, H. & Nisenoff, M. (1986) Defect detection with a SQUID magnetometer *Review of Progress in QNDE 6* (ed) Thompson, D.O. & Chimenti, D. (New York: Plenum) 669-704
- Weinstock, H. (1991). A review of SQUID magnetometry applied to nondestructive evaluation. *IEEE Trans. Mag.*, Vol. 27, No. 2, (March 1991), pp. 3231-3236, ISSN 0018-9464
- Weinstock, H. (Ed.), (1995) *SQUID sensors: Fundamentals, Fabrication and Applications*, Kluwer, ISBN 0-7923-4350-6, Dordrecht

IntechOpen



Nondestructive Testing Methods and New Applications

Edited by Dr. Mohammad Omar

ISBN 978-953-51-0108-6

Hard cover, 264 pages

Publisher InTech

Published online 02, March, 2012

Published in print edition March, 2012

Nondestructive testing enables scientists and engineers to evaluate the integrity of their structures and the properties of their materials or components non-intrusively, and in some instances in real-time fashion. Applying the Nondestructive techniques and modalities offers valuable savings and guarantees the quality of engineered systems and products. This technology can be employed through different modalities that include contact methods such as ultrasonic, eddy current, magnetic particles, and liquid penetrant, in addition to contact-less methods such as in thermography, radiography, and shearography. This book seeks to introduce some of the Nondestructive testing methods from its theoretical fundamentals to its specific applications. Additionally, the text contains several novel implementations of such techniques in different fields, including the assessment of civil structures (concrete) to its application in medicine.

How to reference

In order to correctly reference this scholarly work, feel free to copy and paste the following:

Nagendran Ramasamy and Madhukar Janawadkar (2012). SQUID Based Nondestructive Evaluation, Nondestructive Testing Methods and New Applications, Dr. Mohammad Omar (Ed.), ISBN: 978-953-51-0108-6, InTech, Available from: <http://www.intechopen.com/books/nondestructive-testing-methods-and-new-applications/squid-based-nondestructive-evaluation>

INTECH
open science | open minds

InTech Europe

University Campus STeP Ri
Slavka Krautzeka 83/A
51000 Rijeka, Croatia
Phone: +385 (51) 770 447
Fax: +385 (51) 686 166
www.intechopen.com

InTech China

Unit 405, Office Block, Hotel Equatorial Shanghai
No.65, Yan An Road (West), Shanghai, 200040, China
中国上海市延安西路65号上海国际贵都大饭店办公楼405单元
Phone: +86-21-62489820
Fax: +86-21-62489821

© 2012 The Author(s). Licensee IntechOpen. This is an open access article distributed under the terms of the [Creative Commons Attribution 3.0 License](#), which permits unrestricted use, distribution, and reproduction in any medium, provided the original work is properly cited.

IntechOpen

IntechOpen